NeuroImage: Clinical 20 (2018) 388–397

Contents lists available at ScienceDirect

NeuroImage: Clinical

journal homepage: www.elsevier.com/locate/ynicl

Gray-matter-specific MR imaging improves the detection of epileptogenic zones in focal cortical dysplasia: A new sequence called fluid and white matter suppression (FLAWS)

Xin Chen[a,b,1], Tianyi Qian[b,c,1], Tobias Kober[d,e,f], Guojun Zhang[g], Zhiwei Ren[g], Tao Yu[g], Yueshan Piao[h], Nan Chen[a,b,*], Kuncheng Li[a,b]

[a] Department of Radiology, Xuanwu Hospital, Capital Medical University, Beijing, PR China
[b] Beijing Key Laboratory of Magnetic Resonance Imaging and Brain Informatics, Beijing, PR China
[c] MR Collaborations NE Asia, Siemens Healthcare, Beijing, PR China
[d] Advanced Clinical Imaging Technology, Siemens Healthcare HC CEMEA SUI DI PI, Lausanne, Switzerland
[e] Department of Radiology, University Hospital (CHUV), Lausanne, Switzerland
[f] LTS5, École Polytechnique Fédérale de Lausanne, Lausanne, Switzerland
[g] Department of Functional Neurosurgery, Xuanwu Hospital, Capital Medical University, Beijing, PR China
[h] Department of Pathology, Xuanwu Hospital, Capital Medical University, Beijing, PR China

ARTICLE INFO

Keywords:
Focal cortical dysplasia
Epileptogenic zone
Magnetic resonance imaging
Fluid and white matter suppression sequence

ABSTRACT

Objectives: To evaluate the diagnostic value and characteristic features of FCD epileptogenic zones using a novel sequence called fluid and white matter suppression (FLAWS).

Materials and methods: Thirty-nine patients with pathologically confirmed FCD and good surgery outcomes (class I or II, according to the Engel Epilepsy Surgery Outcome Scale) were retrospectively included in the study. All the patients underwent a preoperative whole-brain MRI examination that included conventional sequences (T2WI, T1WI, two-dimensional (2D) axial, coronal fluid-attenuated inversion recovery [FLAIR]) and FLAWS. An additional 3D-FLAIR MRI sequence was performed in 17 patients. To evaluate the sensitivity and specificity of FLAWS and investigate the cause of false-positives, 36 healthy volunteers were recruited as normal controls. Two radiologists evaluated all the image data. The detection rates of the FCD epileptogenic zone on different sequences were compared based on five criteria: abnormal cortical morphology (thickening, thinning, or abnormally deep sulcus); abnormal cortical signal intensity; blurred gray-white matter junction; abnormal signal intensity of the subcortical white matter, and the transmantle sign. The sensitivity and specificity of FLAWS for detecting the FCD lesions were calculated with the reviewers blinded to all the clinical information, i.e. to the patient identity and the location of the resected regions. To explore how many features were sufficient for the diagnosis of the epileptogenic zones, the frequency of each criterion in the resected regions and their combinations were assessed on FLAWS, according to the results of the assessment when the reviewers were aware of the location of the resected regions. Based on the findings of the 17 patients with an additional 3D-FLAIR scan when the reviewers were aware of the location of the resected regions, quantitative analysis of the regions of interest was used to compare the tissue contrast among 2D-axial FLAIR, 3D-FLAIR, and the FLAWS sequence. Visualization score analysis was used to evaluate the visualization of the five features on conventional, 3D-FLAIR, and FLAWS images. Finally, to explore the reason for false-positive results, a further evaluation of the whole brain FLAWS images was conducted for all the subjects.

Results: The sensitivity and specificity for detecting the FCD lesions on the FLAWS sequence were 71.9% and 71.1%, respectively. When the reviewers were blinded to the location of the resected regions, the detection rate of the FLAWS sequence was significantly higher than that of the conventional sequences (P = 0.00). In the 17 patients who underwent an additional 3D FLAIR scan, no statistically significant difference was found between the FLAWS and the 3D-FLAIR (P = 0.25). All the patients had at least two imaging features, one of which was "the blurred junction of the gray-white matter." The transmantle sign, which is widely believed to be a specific feature of FCD type II, could also be observed in type I on the FLAWS sequence. The relative tissue contrast of FLAWS was higher than that of the 2D-FLAIR with respect to lesion/white matter (WM), deep gray matter (GM)/

* Corresponding author at: No. 45 Chang-Chun St., Xicheng District, Beijing 100053, PR China.
E-mail address: chenzen8057@sina.com (N. Chen).
[1] The first two authors contributed equally to this work.

https://doi.org/10.1016/j.nicl.2018.08.010
Received 4 March 2018; Received in revised form 9 June 2018; Accepted 7 August 2018
Available online 11 August 2018

WM, and cortex/WM (P = 0.00 for all three measures) and higher than that of the 3D-FLAIR with respect to the lesion/WM (P = 0.01). The visualization score analysis showed that the visualization of FLAWS was more enhanced than that of the conventional and 3D-FLAIR images with respect to the blurred junction (P = 0.00 for both comparisons) and the abnormal signal intensity of the subcortical white matter (P = 0.01 for both comparisons). The thin-threadlike signal and individual FCD features outside the epileptogenic regions were considered the primary cause of the false-positive results of FLAWS.

Conclusions: FLAWS can help in the detection of FCD epileptogenic zones. It is recommended that epileptogenic zone on FLAWS be diagnosed based on a combination of two features, one of which should be the "blurred junction of the gray-white matter" in types I and II. In type III, the combination of "the blurred junction of the gray-white matter" with "abnormal signal intensity of subcortical white matter" is recommended.

1. Introduction

Focal cortical dysplasia (FCD) is an underlying cause of seizures in some patients. A complete resection of the epileptogenic zone is critical for eliminating these seizures (Oluigbo et al., 2015; Rowland et al., 2012). As a non-invasive imaging method with multi-contrasts, magnetic resonance imaging (MRI) plays an important role in pre-operative epileptogenic zone localization. However, approximately 22–38% of FCD patients have negative findings on conventional MRI (Kim et al., 2011; Lerner et al., 2009). As the effectiveness of identifying the epileptogenic zones largely depends on the hardware (e.g., field strength) and software (e.g., MR sequences and post-processing methods) of MRI, as well as the experience of the reader and the MR methods (Duncan et al., 2016), improvements in these factors are needed.

In recent years, several new sequences, such as three-dimensional fluid-attenuated inversion recovery (3D FLAIR) (Saini et al., 2010; Tschampa et al., 2015) and 3D double inversion recovery (3D-DIR) (Soares et al., 2016; Wong-Kisiel et al., 2016), have been used to improve the contrast of the cortex. However, the application of these sequences is limited due to several reasons. First, most studies currently show the superiority of the new sequence through measuring quantitative parameters, such as rating the visual score or measuring the signal-to-noise ratio or tissue contrast, on different types of images. Consequently, they only choose visible lesions on the images. Because the primary objective of applying novel sequences in epilepsy is to improve the detection of epileptogenic zones (defined as cortical areas responsible for seizure generation) that cannot be identified using conventional MRI, it is necessary to recruit patients with negative findings on conventional MRI and with good surgery outcomes. Second, although it is widely believed that five typical MRI features can help to visually identify FCD on conventional sequences (Bernasconi et al., 2011), including abnormalities of the cortex (abnormal cortical morphology, signal increase on T2WI) and the subcortical white matter (blurred junction of the gray-white matter, T2 signal increase, and transmantle sign), there is only one study for type II FCD (Mellerio et al., 2012), that has clearly stated how many features are sufficient for the diagnosis of epileptogenic zones on MRI. Third, it may be difficult to identify lesions from false-positive results caused by the techniques themselves, which have too high a sensitivity and a low specificity (Duncan et al., 2016; Woermann and Vezina, 2013).

In this study, we applied in FCD a new sequence known as fluid and white matter suppression (FLAWS) (Tanner et al., 2012). This sequence provides three different high spatial resolution anatomical images in one scan. First, FLAWS acquires two sets of 3D high spatial resolution images at two different inversion times (TI): TI1, which suppresses the white-matter (WM) signal (WM-nulled image), and TI2, which suppresses the cerebrospinal fluid (CSF) signal (CSF-nulled image). Subsequently, a set of synthetic minimum FLAWS-contrast images is calculated based on the two previously mentioned sets of images, and this suppresses both the WM and CSF signals (gray-matter-specific). Because FCD is caused by localized cortical disruptions of neuronal proliferation and organization (Prayson et al., 2002; Taylor et al., 1971), the gray matter-specific images have the potential to improve the visualization of the FCD epileptogenic zones. To our knowledge, there is to date no published research on the application of FLAWS in FCD. The purpose of this study was to explore whether the FLAWS sequence could help in the detection of FCD epileptogenic zones and to facilitate the application of FLAWS in clinical practice.

2. Methods and materials

Thirty-nine patients with pathologically-confirmed FCD were recruited from our Xuanwu Hospital between October 2014 and July 2017 and retrospectively included in this study. Each patient had a preoperative MRI examination including conventional and FLAWS scans. Their surgical outcomes were categorized as class I or II, according to the Engel Epilepsy Surgery Outcome Scale (Engel, 1993), which were defined as good surgery outcomes. An additional pre-operative 3D-FLAIR scan was performed on 17 patients. This study was approved by the Ethics Committee of Xuanwu hospital. Written informed consent was obtained from each participant.

To evaluate the sensitivity and specificity of FLAWS and investigate the cause of any misdiagnoses, healthy volunteers were recruited as normal controls.

Table 1
Scan parameters for the FLAWS, 3D-FLAIR, and conventional sequences.

	FLAWS	3D-FLAIR	2D-FLAIR	2D-FLAIR	T1WI	T2WI	DWI
TR/TE (ms)	5000/2.88	6000/395	8500/85	8500/88	160/3.05	3800/93	5500/90
TI (ms)	TI1/TI2 409/1100	2100	2371.5	2439			
Flip angle (degree)	FA1/FA2 5/5	T2 var	150	150	70	150	90
Matrix	256 × 256	256 × 256	256 × 180	256 × 256	256 × 205	256 × 256	136 × 136
Slices thickness (mm)	1.0	1.0	3.0	3.0	3.0	3.0	3.0
BW (Hz/px)	310	781	287	201	360	219	1598
Orientation	Sagittal	Sagittal	Axial	Coronal	Axial	Axial	Axial
FOV (mm)	256	250	240	230	240	240	240
iPAT	2	2	2	2	2	2	2
Scan time (sec)	657	422	114	104	38	36	40

2D, two-dimensional; 3D, three-dimensional; BW, band width; DWI, diffusion weighted imaging; FLAIR, fluid-attenuated inversion recovery; FLAWS, fluid and white matter suppression; WM, white matter; FOV, field of view; TE, echo time; TI, inversion time; TR, repetition time.

2.1. Data acquisition

The imaging data of all the participants were collected using a MAGNETOM Verio 3.0 T MR scanner (Siemens Healthcare, Erlangen, Germany) with a 12-channel head-neck coil. All the patients underwent conventional MRI protocols, including 2D axial and coronal FLAIR, T2WI, T1WI, and DWI, in addition to FLAWS. Of the 39 recruited patients, an additional T2-SPACE-Dark-Fluid (3D-FLAIR) sequence was applied to 17 patients who were admitted after March 2016. The scan parameters of each sequence are listed in Table 1. The normal control group only underwent FLAWS and 2D axial FLAIR scans. Their scan parameters were consistent with those of the patient group.

2.2. Data analysis

Two experienced radiologists, with ten and thirteen years' experience, respectively, reviewed the images. Differences in assessments between the radiologists were resolved by means of consensus. They identified FCD epileptogenic zones according to the following five imaging features (Bernasconi et al., 2011): (1) abnormal cortical morphology, such as thickening or thinning, defined as a thickening or thinning of at least half of the normal cortex, or abnormal deep sulcus, visible both on T1WI and T2WI sequences in at least two orthogonal planes; (2) abnormal cortical signal intensity; (3) blurred junction of the gray-white matter, defined as visible on at least one sequence and in two orthogonal planes; (4) abnormal signal intensity of subcortical white matter; and (5) transmantle sign, defined as a subcortical funnel-shaped white matter signal intensity change, tapering toward the ventricle (Fig. 1). Among the three types of FLAWS images (WM-nulled, CSF-nulled, and FLAWS contrast image), we only evaluated the detection ability of the FLAWS-contrast image as it is a gray-matter-specific contrast image. The surgically resected regions were considered as the site of the epileptogenic zones and the gold standard of the comparison among sequences, as all the patients had good surgery outcomes.

The evaluation of FLAWS was performed in four steps. Because clinical information obtained from a former step could affect the latter step, the four steps were conducted in the following order. In steps 1 and 2, we referred to the positive criteria of a previous study (Mellerio et al., 2012); images presenting with at least one of the above five characteristics were considered to be positive for FCD:

Step 1: Two reviewers determined whether the image had an abnormal appearance and where lesions were located on FLAWS performed on all the subjects (patients and normal controls). The sensitivity, specificity, positive predictive value, negative predictive value, likelihood ratio positive, and likelihood ratio negative were calculated.

Step 2: To compare the detection rates of different types of MRI scans, reviewers identified FCD lesions in all the patients. In this step, the overall conventional finding was considered to be positive if any type of the conventional images (2D FLAIR/T2WI/T1WI images) had a positive finding. The comparison was performed twice.

First, the reviewers were blinded to the location of the resected regions but were aware of any clinical information such as symptoms, preoperative electroencephalography (EEG), and magnetoencephalography, simulating the preoperative assessment in clinical practice.

Second, the reviewers were aware of the location of the resected regions. Based on the results of the second assessment, a further evaluation about the frequency of each feature in the resected regions and their combination were applied on the FLAWS-contrast images. Moreover, quantitative comparisons were performed in the 17 patients who also underwent a 3D-FLAIR scan: (1) each feature in the resected regions on conventional, 3D-FLAIR, and FLAWS images was rated on a 3-point visualization scale from 0 (no difference) to 2 (marked difference), compared with the contralateral normal appearing side, under the condition that the reviewers were aware of the location of the resected regions. The visualization scores of the five features on the three kinds of images were compared; (2) We also quantitatively compared perceived the relative contrast between different tissues on 2D-axial FLAIR, 3D-FLAIR, and FLAWS images in these 17 patients. The contrast-to-noise ratio (CNR) was measured because the standard deviation of the inhomogeneous air signal outside the object could not be used for the noise in the CNR estimation on parallel imaging (Stehling et al., 2007; Tschampa et al., 2015) such as 3D-FLAIR and FLAWS. We only chose axial rather than coronal FLAIR in 2D FLAIR, as the scanning range of the coronal 2D FLAIR for epilepsy in our hospital is confined to the hippocampus, whereas that of the axial 2D FLAIR encompasses the entire brain. The perceived relative contrast between different tissues was calculated to compare the sequences using the following formula: (mean signal A − mean signal B)/ (mean signal A + mean signal B) (Morakkabati-Spitz et al., 2006), where A represents the

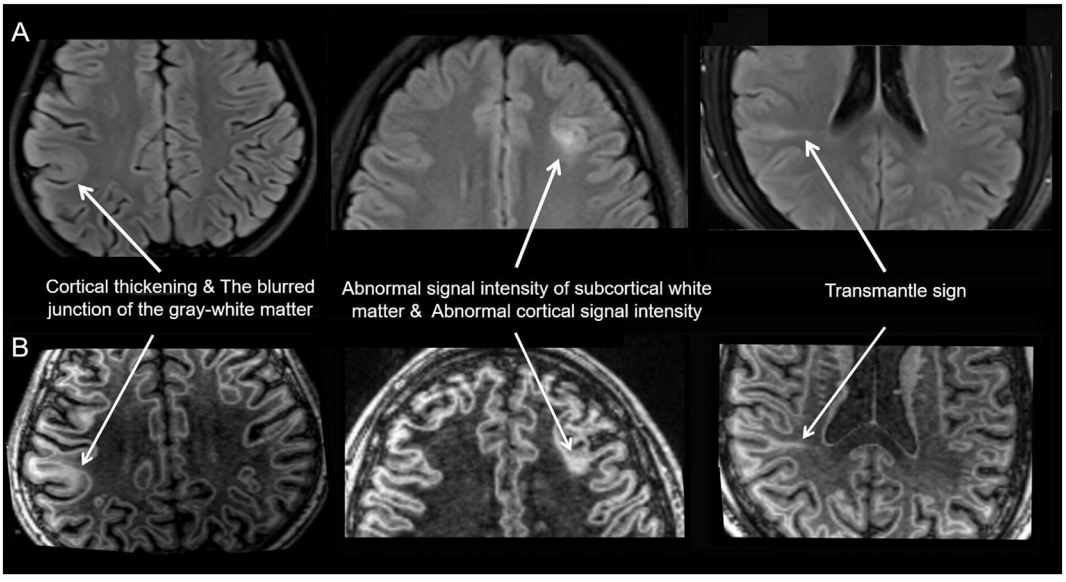

Fig. 1. Sample graphs of five FCD features on the 2D axial FLAIR (A) and the FLAWS contrast image (B).

signal intensity of tissue A, and B represents the signal intensity of tissue B. We defined the corpus callosum (genu) for the white matter, caudate nucleus (head) for deep gray matter, and cortex contralateral to the lesion for normal cortex. The lesion was measured based on the findings when reviewers were aware of the location of the resected regions. The region of interest (ROI) was manually drawn and saved on the FLAWS-contrast image. Three measurements were performed per anatomical site, and the mean values of the ROI measurements were subsequently used. To compare different types of images in the same slice, both 3D-FLAIR and 2D-axial FLAIR images were co-registered to the FLAWS-contrast image using SPM12 of MATLAB, and the same ROIs that had been saved on the FLAWS-contrast image were used in the two types of images.

Step 3: To investigate the reason for false-positive findings, a further reading of the FLAWS images in all the subjects was conducted by the reviewers, when they were aware of who the patients were and where the resected regions were located. If there were some signals like the FCD features, their relationship with age, sex, and location would be explored. In addition, their morphological differences with FCD features would be compared by rating them on a 3-point visualization scale from 0 (no difference) to 2 (marked difference).

Step 4: To establish and optimize the diagnostic criteria of FCD on FLAWS-contrast images, the frequency of the features in the resected regions and the false-positive findings were comprehensively considered together to determine how many features were sufficient for the diagnosis of any epileptogenic zones.

2.3. Statistical methods

Statistical analyses were performed using SPSS 18.0 for Windows (SPSS Inc., Chicago, IL, USA). For statistical comparisons of independent data, the Fisher's exact test was performed. For comparisons of paired binary data, the McNemar test was performed, and for comparisons of multiple data, the Friedman test was conducted. $P < 0.05$ was regarded as being statistically significant. If the result of the Friedman test was statistically significant, a post hoc analysis with Wilcoxon signed-rank tests was conducted with a Bonferroni correction applied, with a new significance level of $0.05/3 \approx 0.02$.

3. Results

The detailed clinical profiles of the patients are summarized in Table 2. Thirty-nine patients (24 male; mean age, 23.3 ± 8.8 years; age range, 8–48 years) were enrolled. According to the Blümcke classification (Blümcke et al., 2011), 21 cases were FCD type I, 11 were FCD

Table 2
The clinical profiles of the FCD patients and their MRI visual evaluation results.

No	Sex	Age (years)	Course (years)	Engle scale	Follow-up (years)	Conventional[a] MRI	3D FLAIR[a]	FLAWS		Resection areas	FCD type
								Blinded	Unblinded		
1	M	29	17	I	3	−	NA	+	+	R Front	Ib
2	F	17	17	I	2.5	−	NA	+	+	R Hipp & Temp	IIa
3	F	18	7	I	2.4	−	NA	+	+	R Temp & Ins	Ib
4	M	27	17	I	2.3	+	NA	+	+	L Front	Ib
5	M	27	6	I	1.6	−	−	+	+	L Hipp & Temp	Ia
6	M	11	10	II	1.7	−	NA	+	+	R Hipp & Temp & Front	Ia
7	M	21	5	II	2	−	NA	+	+	R Front	IIa
8	M	24	21	I	2.7	+	NA	+	+	L Front	IIa
9	M	16	7	I	1.6	+	+	+	+	L Pari	IIb
10	M	8	6	II	1.5	−	−	−	+	L Temp & Occi & Pari	Ia
11	M	29	24	I	1.5	+	+	+	+	R Temp & Front	Ic
12	M	34	14	I	2.5	−	NA	−	+	L Hipp & Temp	IIIa
13	F	8	1	II	3	+	NA	+	+	R Temp & Occi	Ib
14	M	48	16	I	1.7	−	+	+	+	L Front	Ic
15	M	23	6	I	1.9	+	+	+	+	L Hipp & Temp	Ia
16	F	24	2	II	2.4	−	NA	+	+	R Hipp & Temp	Ia
17	M	24	10	I	2.4	−	NA	−	−	L Hipp & Temp	Ia
18	F	25	13	I	2.5	−	NA	−	−	L Hipp & Temp & Front	Ia
19	F	38	37	I	2.3	+	NA	+	+	R Front	IIb
20	F	42	30	I	1.1	−	−	−	+	R Pari	Ia
21	M	10	4	I	1.4	−	NA	+	+	R Front	Ib
22	F	19	8	I	1.3	−	−	−	+	L Temp & Occi	Ic
23	F	23	10	I	2.8	+	NA	+	+	R Hipp & Temp	IIa
24	M	26	14	I	1.1	−	+	+	+	R Front	IIa
25	M	12	2	I	2.5	+	NA	+	+	R Front	IIb
26	M	20	8	I	2.4	+	NA	+	+	R Hipp & Temp	IIb
27	F	25	19	I	3.2	+	NA	+	+	L Front	IIb
28	F	19	14	I	2.4	+	NA	+	+	R Hipp & Temp	IIIa
29	M	29	14	I	2	−	−	−	−	L Hipp & Temp	IIIa
30	M	34	30	I	1.9	+	+	+	+	L Hipp & Temp	IIIa
31	M	17	10	II	1.5	−	−	−	−	R Temp	Ia
32	M	13	8	II	0.5	+	+	+	+	R Pari	IIIa
33	M	19	12	I	0.3	−	−	+	+	L Hipp & Temp & Front	Ib
34	F	23	10	I	0.3	−	−	−	−	L Temp & Occi & Pari	Ib
35	F	23	21	I	0.3	−	−	+	+	R Hipp & Temp	IIIa
36	F	25	17	II	2.7	−	NA	−	−	L Temp & Occi & Pari	Ia
37	M	20	17	II	2	−	NA	−	+	R Front	Ia
38	F	25	5	I	2.6	−	NA	+	+	R Front	IIa
39	M	35	6	II	1.1	+	+	+	+	R Hipp & Temp	IIIb

[a] The results were same whether the reviewers were blinded to the location of the resection regions or not; Blinded, the reviewers were blinded to the location of the resection regions; Unblinded, the reviewers were not blinded to the location of the resection regions; F, female; FCD, frontal cortical dysplasia; Front, frontal lobe; Hipp, hippocampus; Ins, insula; L, left; M, male; Occi, occipital lobe; Pari, parietal lobe; R, right; Temp, temporal lobe; +, positive; −, negative; NA, not applicable.

type II, and 7 were FCD type III. Thirty-five had more than one-year postoperative follow-up, whereas the remaining four had less than six-month follow-up. A total of 36 normal controls (20 men; mean age, 24.8 ± 7.5 years; age range, 10–50 years) were enrolled. No structural abnormality was found on 2D axial FLAIR in this group. No significant differences were observed with respect to sex (P = 0.56) or age (P = 0.27) between the patients and normal controls. In addition, none had any previous neurological disease.

3.1. The operation of FLAWS when the reviewers were blinded to any information

The numbers of true positives, false-positives, true negatives, and false-negatives were 23 (13 had positive conventional MRI results), 11 (7 were patients), 27, and 9, respectively. The sensitivity, specificity, positive predictive value, negative predictive value, likelihood ratio positive, and likelihood ratio negative were 71.9%, 71.1%, 67.6%, 75.0%, 2.48, and 0.40, respectively.

3.2. The detection rates of different types of MRI scans in patients

Among the 39 patients, 24 had negative findings on the conventional images when the reviewers were blinded to the location of the resected regions; of these, 17 were FCD type I, 4 FCD type II, and 3 FCD type III. In addition, of the 24 patients, 13 negative findings were positive on FLAWS, 8 of whom were FCD type I, 4 FCD type II, and 1 FCD type III. The detection rate of FLAWS was significantly higher than that of the conventional sequences (P = 0.00). When the reviewers were aware of the location of the resected regions, no additional lesions could be detected on the conventional images, whereas five more negative findings were positive on FLAWS, 4 of whom were FCD type I and 1 FCD type III.

Among the 17 patients who additionally underwent the 3D-FLAIR scan, 9 patients had negative findings when the reviewers were blinded to the location of the resected regions; 7 were FCD type I and 2 FCD type III. Of the 9 patients, 3 negative findings were positive on FLAWS, 2 of whom were FCD type I and 1 FCD type III (Figs. 2 and 3). However, no statistically significant difference was found between FLAWS and 3D-FLAIR (P = 0.25). When the reviewers were aware of the location of the resected regions, no additional lesions could be detected on the 3D-FLAIR whereas three more negative findings were positive on FLAWS, all FCD type I.

The visualization score analysis showed the following: (1) there were no significant differences among FLAWS, 3D-FLAIR, or the conventional images with respect to abnormal cortical morphology (P = 0.42) and abnormal cortical signal intensity (P = 0.85); (2) the visualization of FLAWS was more enhanced than that of the conventional and 3D-FLAIR images with respect to the blurred junction (P = 0.00 for both comparisons) and the abnormal signal intensity of the subcortical white matter (P = 0.01 for both comparisons); (3) although there was a difference among FLAWS, 3D-FLAIR, and the conventional images with respect to the transmantle sign (P = 0.04) (Fig. 2B, Table S1), no statistical difference was found between any two of the studies (P = 0.05 for FLAWS vs. 3D-FLAIR, and P = 0.06 for FLAWS vs. conventional images).

When measuring the tissue contrast, 14 of the 17 patients had positive lesions on the FLAWS-contrast images when the reviewers were aware of the location of the resected regions. There was no significant difference between the 2D versus 3D FLAIR sequences (P > 0.02). The relative tissue contrast of FLAWS was higher than that of the 2D with respect to lesion/WM, deep gray matter (GM)/WM, and cortex/WM (P = 0.00 for all three) and higher than that of 3D FLAIR with respect to lesion/WM (P = 0.01) (Table 3).

3.3. Five FCD features on FLAWS images in the epileptogenic zones

In patients with positive findings on FLAWS when the reviewers were aware of the location of resected regions (n = 33), 16 were FCD type I, 11 were FCD type II, and 6 were FCD type III. All the patients had at least two features, one of which was “the blurred junction of the gray-white matter.” In addition, the transmantle sign could be detected in 16 of the 39 patients, and it was not limited to type II patients (Figs. 2A, 4, and 5).

3.4. Reasons for false-positives

In all the normal controls and patients, more than one thin-threadlike signal could be detected in the subcortical white matter on FLAWS, but not on FLAIR. It appeared alone without any other kinds of abnormal signals in the surrounding area. Its morphological characteristics could easily be confused with the transmantle sign. Both extended from the ventricle to the cortex, exhibiting a hypointense signal on the CSF-nulled image and a hyperintense signal on the WM-nulled and FLAWS contrast images (Fig. 6). The degrees of thickness, length, and clarity between the thin-threadlike signal and the transmantle sign were not significantly different (P > 0.05). No correlation

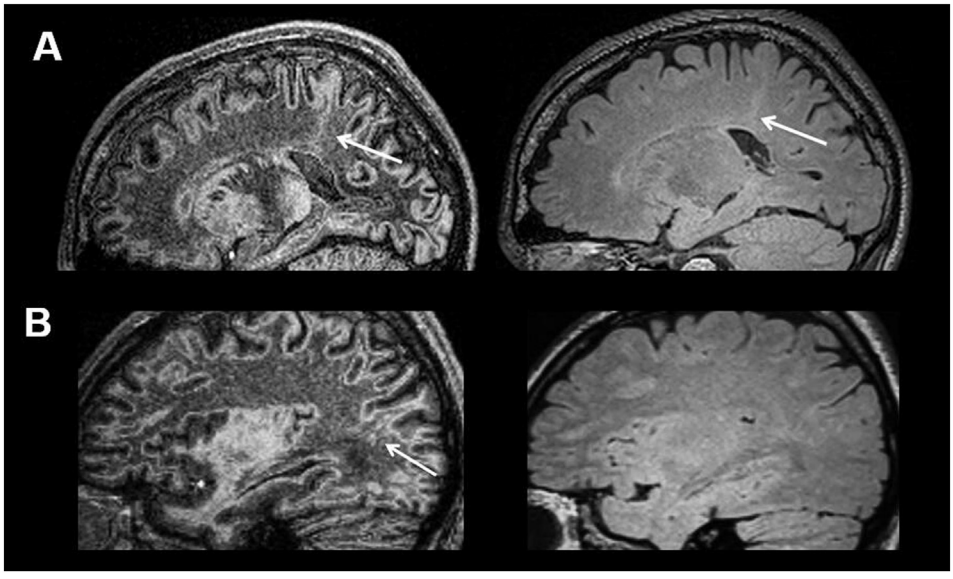

Fig. 2. Epileptogenic lesions on 3D-FLAIR and FLAWS. In patient No. 9 (FCD type IIb), the lesion, including “the transmantle sign” (arrow), “thickening cortex,” and “blurred junction of the gray-white matter,” is more visible on the FLAWS than the 3D-FLAIR image (A). In patient No.22 (FCD type Ic), the lesion, including “the transmantle sign” (arrow) and “abnormal signal intensity of subcortical white matter,” could be found on the FLAWS image, not on the 3D-FLAIR image (B).

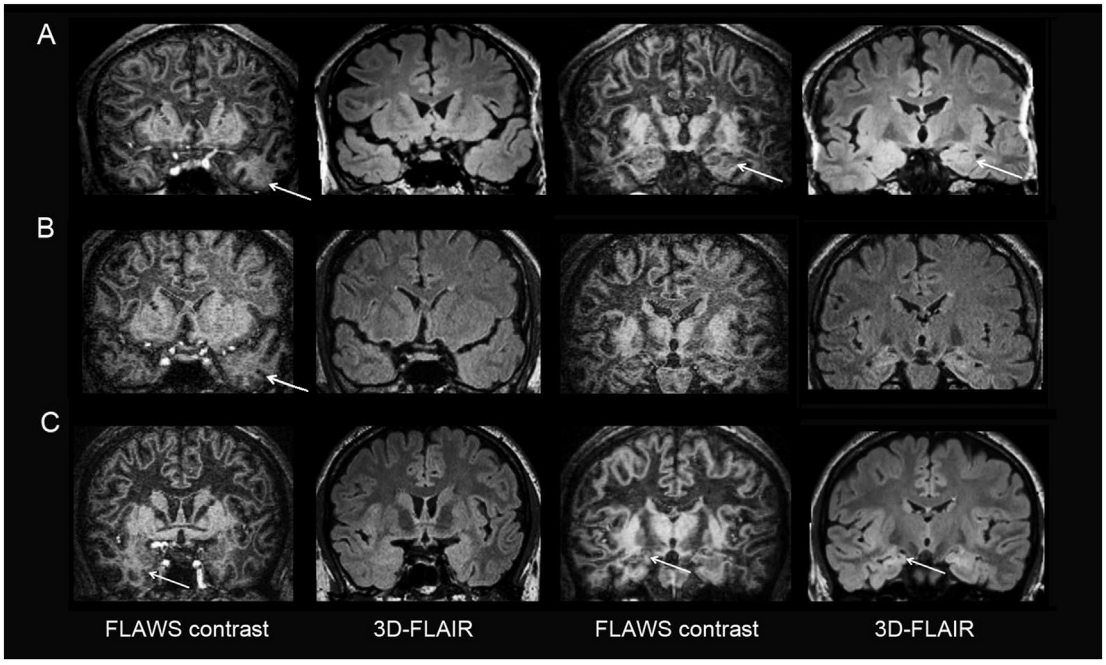

Fig. 3. Patients with 3D-FLAIR-negative but FLAWS-positive findings. The decreased volume of the hippocampus (A and C) or temporal horn (B) could be detected on both 3D-FLAIR and FLAWS but was more obvious on 3D-FLAIR. However, FCD features, including "blurred junction of the gray-white matter" and "abnormal signal intensity of subcortical white matter," could only be observed on FLAWS in their epileptogenic lesions. In patient No.5 (FCD type Ia), the epileptogenic lesion was in the left hippocampus and temporal lobe (A). In patient No.33 (FCD type Ib), the epileptogenic lesion was in the left hippocampus, temporal lobe, and frontal lobe (B). In patient No.35 (FCD type IIIa), the epileptogenic lesion was in the right hippocampus and temporal lobe (C).

Table 3
The quantitatively comparison of perceived relative contrast in 14 patients with positive lesions on FLAWS when reviewers were aware of the location of the resection regions.

	Sequence			P*	P** for post hoc		
	2D FLAIR	3D FLAIR	FLAWS		2D vs 3D FLAIR	2D FLAIR vs FLAWS	3D FLAIR vs FLAWS
Lesion/WM	0.07 ± 0.22	0.05 ± 0.10	0.21 ± 0.13	0.02	0.38	0.01	0.00
Deep GM/WM	0.08 ± 0.19	0.09 ± 0.05	0.31 ± 0.10	0.00	0.25	0.00	0.00
Cortex/WM	0.13 ± 0.24	0.08 ± 0.10	0.27 ± 0.11	0.00	0.29	0.05	0.00

* $P < 0.05$ was considered significant (two-tailed).
** $P < 0.02$ was considered significant (one-tailed). WM, white matter; GM, gray matter.

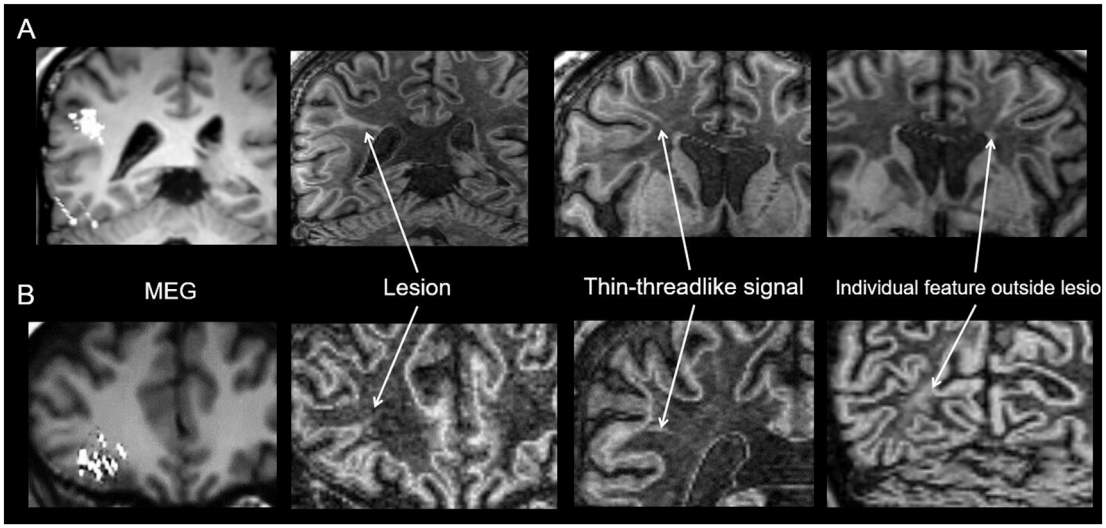

Fig. 4. Patient No.26 (FCD type IIb) (A) and patient No.3 (FCD type Ib) (B). The first column shows the MEG results which are consistent with the resected regions; the following three columns show the "transmantle sign" in the epileptogenic lesion, the thin-threadlike signal, and individual FCD features outside the epileptogenic regions on the FLAWS contrast image, respectively.

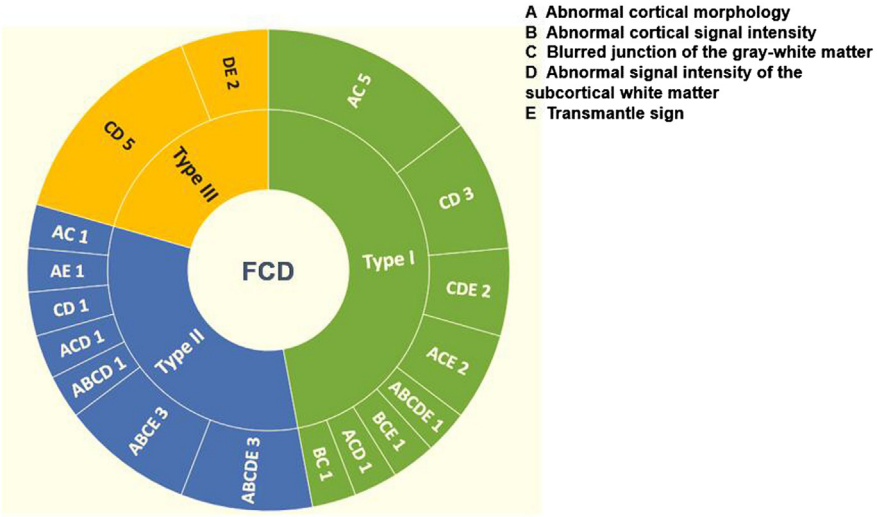

Fig. 5. Five criteria in three FCD types on the FLAWS images. Letters A to E correspond to five FCD criteria, respectively. The outer ring shows the combination patterns of the five criteria and the number of patterns.

was observed between the thin-threadlike signal and the transmantle sign with respect to sex, age, or location in both the patients and normal controls ($P > 0.05$).

In the patients, individual FCD features could occasionally be found outside the epileptogenic regions, contralateral or ipsilateral to the epileptogenic zone (Fig. 4).

3.5. Tailored visual criteria for FLAWS

To minimize the false-positive findings when recalculating the frequency of each feature and their combination in the epileptogenic lesions, the transmantle sign was excluded and the epileptogenic lesions were required to have more than two of the other four features.

The most frequent feature was “the blurred junction of the gray-white matter” in both types I and II. This was accompanied by any of the other three features in 100% type I and 90.9% II patients. In type III, “the blurred junction of the gray-white matter” with “abnormal signal intensity of the subcortical white matter” was the only combination seen (71.4%).

4. Discussion

The primary findings of the FLAWS sequence in patients with histologically-confirmed FCD and good surgery outcomes were as follows: (1) the detection rate of the FLAWS sequence was higher than that of conventional sequences and 3D-FLAIR; (2) all three FCD types had at least two features on FLAWS, one of which was “blurred junction of the gray-white matter;” (3) false-positive results were primarily caused by the thin-threadlike signal and individual FCD feature outside the epileptogenic regions; and (4) the transmantle sign was not a specific criterion of FCD type II on FLAWS.

4.1. The feasibility of FLAWS for clinical application in FCD

Based on the MP2RAGE sequence, the FLAWS sequence acquires two gradient echo readout trains at TI1 and TI2 in one acquisition (Marques et al., 2010). Tanner and colleagues (Tanner et al., 2012) reported that the MP2RAGE sequence can generate two images at a TI1 of 409 ms and TI2 of 1100 ms on a 3 T MR scanner, including one WM-

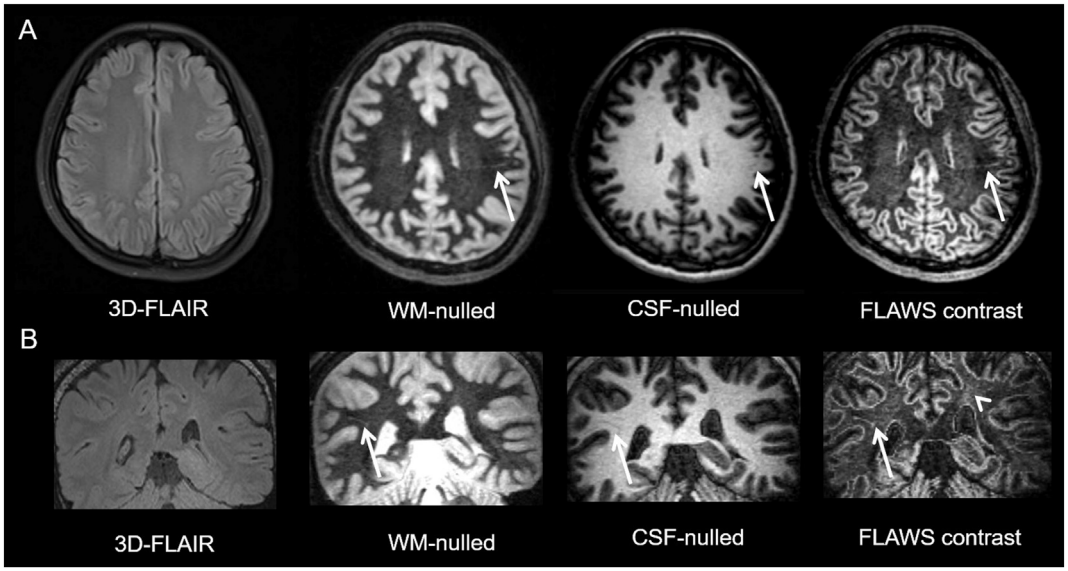

Fig. 6. The thin-threadlike signal (arrow) in a 28-year-old female normal control (A) and a 16-year-old male FCD type II patient (B), respectively. The thin-threadlike signal is invisible on the FLAIR and visible on the FLAWS images. The arrow head points to the epileptogenic zone of the patient.

nulled image and one CSF-nulled image. They also proposed a minimum intensity projection between the two contrasts (FLAWS contrast image), resulting in a gray-matter specific image. To our knowledge, the FLAWS sequence has been previously used once as an experimental sequence in five healthy volunteers for future application in deep brain stimulation placement (Tanner et al., 2012). The present study is the first that investigated the FLAWS sequence in patients with FCD.

The improved visualization of epileptogenic zones on FLAWS is primarily due to the following factors: (1) gray matter-specific contrast is suitable for displaying the predominant histopathological abnormalities in subtle epileptogenic zones, including altered cortical organization and cytological anomalies at the bottom of the sulcus (Bernasconi et al., 2011; Blümcke et al., 2011). It is consistent with our results that the most common feature of FCD was "blurred junction of the gray-white matter;" (2) the 1-mm isotropic voxel size can increase the spatial resolution and reduce partial volume effects (Kokkinos et al., 2017); (3) the epileptogenic zones at the bottom of the sulcus, which cannot be detected in the 2D images, can be displayed well by using multi-planar reformatting of 3D images. According to our results, some epileptogenic lesions, which cannot be identified on conventional MRI or even on 3D-FLAIR images, could be detected on the FLAWS images. This may provide surgical opportunities for more patients, particularly for type I patients who are more likely to have negative MR results (Bernasconi et al., 2011; Seo et al., 2011).

One disadvantage of FLAWS is that its acquisition time is longer than that of both the conventional and 3D-FLAIR sequences. The basic protocol for patients with epilepsy, established by the International League Against Epilepsy (1997), includes whole-brain T1WI/T2WI with the minimum slice thickness possible in two orthogonal planes and a volumetric (1 mm isotropic voxels) 3D-T1WI. The total acquisition time to complete the basic protocol is the same or greater than that of FLAWS. This suggests that FLAWS may be useful for some clinical applications.

4.2. Reasons for false-positive and false-negative results and the interpretation criteria for FCD epileptogenic zone on FLAWS

False-positive results are primarily caused by the thin-threadlike signal and individual FCD features outside the epileptogenic regions, for the following reasons:

(1) The morphological characteristics of the thin-threadlike signal can be confused with the transmantle sign. Based on its morphological and signal characteristics, the thin-threadlike signal may be most likely type II Virchow-Robin (VR) spaces (Kwee and Kwee, 2007; Tsutsumi et al., 2011). Although small VR spaces (< 2 mm) can appear in all age groups, their visualization using MRI is dependent on the applied imaging technique (Pantoni et al., 2005). Higher signal-to-noise ratios (SNR) at higher magnetic field strengths, which are all advantages of the FLAWS sequence (high resolution, thin-slice, multi-planar reformatting), can also improve the visualization of the VR spaces. In the FCD epileptogenic zones, the thin-threadlike signal could be distinguished from the transmantle sign, as the thin-threadlike signal appears alone whereas the transmantle sign in the epileptogenic zone was always accompanied by at least one of the other four FCD features on FLAWS. However, outside the epileptogenic zone, it is difficult to distinguish them as the transmantle sign could also appear alone;

(2) The clinical significance of individual FCD features outside the epileptogenic regions is unclear. According to previous structural MRI studies, diffuse structural changes can be found outside the epileptogenic regions, suggesting an anatomical and functional network mechanism linked to the epileptogenic zone (Bonilha et al., 2006; Colliot et al., 2006; Doucet et al., 2015; Keller et al., 2002) or occult dysplastic epileptogenic zones (Najm et al., 2013; Prayson et al., 2002; Rugg-Gunn et al., 2006). The fact that our patients had good outcomes supports the notion that the individual FCD features outside the epileptogenic regions are a component of the epilepsy network rather than the epileptogenic zone. Although the role of features in the epileptogenic zones and individual FCD features outside the epileptogenic zones are different, their morphological characters might be the same. Thus, individual FCD features outside the epileptogenic zones cannot be distinguished from those in the epileptogenic zones on FLAWS; if we continue to follow the previous criteria, that finding is positive, provided any one of the five features is present.

False-negative results are primarily caused by insufficient clinical information (subjective factor) and limitations of the current FLAWS technology (objective factor). The subjective factor is supported by the fact that some negative lesions on FLAWS in the simulated preoperative assessment were positive when the reviewers were aware of the location of the resection regions. The limitations of the current FLAWS technology may be the reason that there were some lesions that could not be found or detected, even when the reviewers were aware of the location of the resected regions. Improvements in the MR hardware technology, such as higher-field magnets at > 3 T, combined with the use of head coils with more phased arrays, may be helpful (Bernasconi et al., 2011; Duncan et al., 2016).

Overall, to minimize false-positives caused by the thin-threadlike signal and the individual FCD feature outside the epileptogenic regions, a tailored criterion is proposed, namely, that the interpretation should be performed in the context of clinical information, which can guide the reviewers to find lesions in the most likely places to improve the detection rate, and diagnosis of the epileptogenic lesions should be based on a combination of two features, one of which is "the blurred junction of the gray-white matter."

4.3. The transmantle sign was not specific for FCD type II on FLAWS

One notable finding of our study was that the transmantle sign was not specific for FCD type II on FLAWS. We determined that subcortical funnel-shaped signals in the epileptogenic zone signified the transmantle sign rather than the thin-threadlike signal or some other structure; the thin-threadlike signal appeared alone, whereas at least two features could be found in the epileptogenic zones.

The high-resolution, thin-slice (1.0 mm) and multi-planar reformatting of the FLAWS sequence can help radiologists identify the transmantle sign (Kokkinos et al., 2017). According to our findings, the transmantle sign could be seen in types I and II on FLAWS, which is not consistent with previous studies demonstrating that the transmantle sign on conventional sequences is specific to FCD type II (Kaido et al., 2012; Kokkinos et al., 2017; Muhlebner et al., 2012; Sakakibara et al., 2012). This finding may expand our understanding of the imaging criteria and corresponding pathological basis of FCD. According to the Blümcke classification (Blümcke et al., 2011), neocortical dyslamination exists in both types I and II, whereas dysmorphic neurons and balloon cells only exist in FCD types IIa and IIb, respectively. Because the transmantle sign can be found in both types I and II, its pathology is more likely related to abnormal cortical layers than to dysmorphic neurons and balloon cells. This inference is supported by a pathology-based study that demonstrated that various layer-specific markers were abnormally present and continuously distributed in the neurons of the transmantle dysplasia epileptogenic zone (Sakakibara et al., 2012) and by a clinical retrospective study showing the transmantle sign in a patient with FCD type I (Wang et al., 2013a). Because the presence of the transmantle sign is associated with highly favorable seizure outcomes (Wang et al., 2013a, b), its enhanced visualization may improve the process for selection of candidates for surgery.

4.4. Limitations

There are several limitations in our study. First, it was retrospective and was only based on patients who underwent surgeries that had a good outcome, which does not represent the entire spectrum of FCD. However, a study on the detection of the epileptogenic zone would be limited if patients do not have histological confirmation and post-operative follow-up. Future studies should continue to retrospectively recruit patients with histological confirmation but poor outcome to explore whether the five features have any differences in their morphological characteristics, frequency, or a combination. Second, the small sample size of patients with the 3D-FLAIR scan may be the reason for the lack of a statistically significant difference between FLAWS and 3D-FLAIR. Further studies with larger sample sizes should therefore be conducted. Third, the positive MRI findings were only based on conventional visual analysis. Automatic quantitative analysis, such as voxel-based morphometry, would possibly further increase the detection rate (Wang et al., 2016). Unfortunately, the post-processing methods have not been used in routine practice and their interpretation still requires experienced readers (Wang and Alexopoulos, 2016). Finally, future studies should compare the FLAWS sequence to other advanced sequences, such as the double inversion recovery sequence (Wong-Kisiel et al., 2016), in which both the CSF and WM signals can be suppressed. Even if the detection rates of the two sequences are similar, the advantage of producing three perfectly registering, 3D high spatial resolution structural images makes the FLAWS sequence more practical for FCD.

5. Conclusion

In conclusion, the FLAWS sequence can help detect epileptogenic FCD lesions. Diagnosis of the epileptogenic focus should be based on a combination of two features, one of which is the “blurred junction of the gray-white matter.” The transmantle sign is not specific for FCD type II on FLAWS, indicating that the pathology of the transmantle sign is more likely related to abnormal cortical layers than dysmorphic neurons and balloon cells, which may expand the current understanding of the imaging criteria and corresponding pathological basis of FCD.

Supplementary data to this article can be found online at https://doi.org/10.1016/j.nicl.2018.08.010.

Acknowledgements

The authors would like to thank Duanyu Ni, Chang Liu, and Xi Zhang for their assistance in the recruitment of patients.

This work was supported by a grant from the Beijing Municipal Administration of Hospitals Clinical Medicine Development of Special Funding Support (code ZYLX201609); the Beijing Municipal Science and Technology Commission (code Z171100000117001); and the Capital Health Research and Development of Special Project (code 2016-1-2011).

References

Bernasconi, A., Bernasconi, N., Bernhardt, B.C., Schrader, D., 2011. Advances in MRI for ‘cryptogenic’ epilepsies. Nat. Rev. Neurol. 7, 99–108.

Blümcke, I., Thom, M., Aronica, E., Armstrong, D.D., Vinters, H.V., Palmini, A., Jacques, T.S., Avanzini, G., Barkovich, A.J., Battaglia, G., Becker, A., Cepeda, C., Cendes, F., Colombo, N., Crino, P., Cross, J.H., Delalande, O., Dubeau, F., Duncan, J., Guerrini, R., Kahane, P., Mathern, G., Najm, I., Ozkara, C., Raybaud, C., Represa, A., Roper, S.N., Salamon, N., Schulze-Bonhage, A., Tassi, L., Vezzani, A., Spreafico, R., 2011. The clinicopathologic spectrum of focal cortical dysplasias: a consensus classification proposed by an ad hoc Task Force of the ILAE Diagnostic Methods Commission. Epilepsia 52, 158–174.

Bonilha, L., Montenegro, M.A., Rorden, C., Castellano, G., Guerreiro, M.M., Cendes, F., Li, L.M., 2006. Voxel-based morphometry reveals excess gray matter concentration in patients with focal cortical dysplasia. Epilepsia 47, 908–915.

Colliot, O., Bernasconi, N., Khalili, N., Antel, S.B., Naessens, V., Bernasconi, A., 2006. Individual voxel-based analysis of gray matter in focal cortical dysplasia. NeuroImage 29, 162–171.

Doucet, G.E., He, X., Sperling, M., Sharan, A., Tracy, J.I., 2015. Frontal gray matter abnormalities predict seizure outcome in refractory temporal lobe epilepsy patients. Neuroimage Clin. 9, 458–466.

Duncan, J.S., Winston, G.P., Koepp, M.J., Ourselin, S., 2016. Brain imaging in the assessment for epilepsy surgery. Lancet Neurol. 15, 420–433.

Engel Jr., J., 1993. Update on surgical treatment of the epilepsies. Summary of the second International Palm Desert Conference on the surgical treatment of the epilepsies (1992). Neurology 43, 1612–1617.

Recommendations for neuroimaging of patients with epilepsy. Commission on Neuroimaging of the International League Against Epilepsy. Epilepsia 38, 1255–1256.

Kaido, T., Otsuki, T., Kakita, A., Sugai, K., Saito, Y., Sakakibara, T., Takahashi, A., Kaneko, Y., Saito, Y., Takahashi, H., Honda, R., Nakagawa, E., Sasaki, M., Itoh, M., 2012. Novel pathological abnormalities of deep brain structures including dysplastic neurons in anterior striatum associated with focal cortical dysplasia in epilepsy. J. Neurosurg. Pediatr. 10, 217–225.

Keller, S.S., Wieshmann, U.C., Mackay, C.E., Denby, C.E., Webb, J., Roberts, N., 2002. Voxel based morphometry of grey matter abnormalities in patients with medically intractable temporal lobe epilepsy: effects of side of seizure onset and epilepsy duration. J. Neurol. Neurosurg. Psychiatry 73, 648–655.

Kim, Y.H., Kang, H.C., Kim, D.S., Kim, S.H., Shim, K.W., Kim, H.D., Lee, J.S., 2011. Neuroimaging in identifying focal cortical dysplasia and prognostic factors in pediatric and adolescent epilepsy surgery. Epilepsia 52, 722–727.

Kokkinos, V., Kallifatidis, A., Kapsalaki, E.Z., Papanikolaou, N., Garganis, K., 2017. Thin isotropic FLAIR MR images at 1.5 T increase the yield of focal cortical dysplasia transmantle sign detection in frontal lobe epilepsy. Epilepsy Res. 132, 1–7.

Kwee, R.M., Kwee, T.C., 2007. Virchow-Robin spaces at MR imaging. Radiographics 27, 1071–1086.

Lerner, J.T., Salamon, N., Hauptman, J.S., Velasco, T.R., Hemb, M., Wu, J.Y., Sankar, R., Donald Shields, W., Engel Jr., J., Fried, I., Cepeda, C., Andre, V.M., Levine, M.S., Miyata, H., Yong, W.H., Vinters, H.V., Mathern, G.W., 2009. Assessment and surgical outcomes for mild type I and severe type II cortical dysplasia: a critical review and the UCLA experience. Epilepsia 50, 1310–1335.

Marques, J.P., Kober, T., Krueger, G., van der Zwaag, W., Van de Moortele, P.F., Gruetter, R., 2010. MP2RAGE, a self bias-field corrected sequence for improved segmentation and T1-mapping at high field. NeuroImage 49, 1271–1281.

Mellerio, C., Labeyrie, M.A., Chassoux, F., Daumas-Duport, C., Landre, E., Turak, B., Roux, F.X., Meder, J.F., Devaux, B., Oppenheim, C., 2012. Optimizing MR imaging detection of type 2 focal cortical dysplasia: best criteria for clinical practice. AJNR Am. J. Neuroradiol. 33, 1932–1938.

Morakkabati-Spitz, N., Gieseke, J., Kuhl, C., Lutterbey, G., von Falkenhausen, M., Traber, F., Park-Simon, T.W., Zivanovic, O., Schild, H.H., 2006. MRI of the pelvis at 3 T: very high spatial resolution with sensitivity encoding and flip-angle sweep technique in clinically acceptable scan time. Eur. Radiol. 16, 634–641.

Muhlebner, A., Coras, R., Kobow, K., Feucht, M., Czech, T., Stefan, H., Weigel, D., Buchfelder, M., Holthausen, H., Pieper, T., Kudernatsch, M., Blumcke, I., 2012. Neuropathologic measurements in focal cortical dysplasias: validation of the ILAE 2011 classification system and diagnostic implications for MRI. Acta Neuropathol. 123, 259–272.

Najm, I., Jehi, L., Palmini, A., Gonzalez-Martinez, J., Paglioli, E., Bingaman, W., 2013. Temporal patterns and mechanisms of epilepsy surgery failure. Epilepsia 54, 772–782.

Oluigbo, C.O., Wang, J., Whitehead, M.T., Magge, S., Myseros, J.S., Yaun, A., Depositario-Cabacar, D., Gaillard, W.D., Keating, R., 2015. The influence of lesion volume, perilesion resection volume, and completeness of resection on seizure outcome after resective epilepsy surgery for cortical dysplasia in children. J. Neurosurg. Pediatr. 15, 644–650.

Pantoni, L., Basile, A.M., Pracucci, G., Asplund, K., Bogousslavsky, J., Chabriat, H., Erkinjuntti, T., Fazekas, F., Ferro, J.M., Hennerici, M., O'Brien, J., Scheltens, P., Visser, M.C., Wahlund, L.O., Waldemar, G., Wallin, A., Inzitari, D., 2005. Impact of age-related cerebral white matter changes on the transition to disability – the LADIS study: rationale, design and methodology. Neuroepidemiology 24, 51–62.

Prayson, R.A., Spreafico, R., Vinters, H.V., 2002. Pathologic characteristics of the cortical dysplasias. Neurosurg. Clin. N. Am. 13 (17–25), vii.

Rowland, N.C., Englot, D.J., Cage, T.A., Sughrue, M.E., Barbaro, N.M., Chang, E.F., 2012. A meta-analysis of predictors of seizure freedom in the surgical management of focal cortical dysplasia. J. Neurosurg. 116, 1035–1041.

Rugg-Gunn, F.J., Boulby, P.A., Symms, M.R., Barker, G.J., Duncan, J.S., 2006. Imaging the neocortex in epilepsy with double inversion recovery imaging. NeuroImage 31, 39–50.

Saini, J., Singh, A., Kesavadas, C., Thomas, B., Rathore, C., Bahuleyan, B., Radhakrishnan, A., Radhakrishnan, K., 2010. Role of three-dimensional fluid-attenuated inversion recovery (3D FLAIR) and proton density magnetic resonance imaging for the detection and evaluation of lesion extent of focal cortical dysplasia in patients with refractory epilepsy. Acta Radiol. 51, 218–225.

Sakakibara, T., Sukigara, S., Saito, T., Otsuki, T., Takahashi, A., Kaneko, Y., Kaido, T., Saito, Y., Sato, N., Kimura, Y., Nakagawa, E., Sugai, K., Sasaki, M., Goto, Y., Itoh, M., 2012. Delayed maturation and differentiation of neurons in focal cortical dysplasia with the transmantle sign: analysis of layer-specific marker expression. J. Neuropathol. Exp. Neurol. 71, 741–749.

Seo, J.H., Holland, K., Rose, D., Rozhkov, L., Fujiwara, H., Byars, A., Arthur, T., DeGrauw, T., Leach, J.L., Gelfand, M.J., Miles, L., Mangano, F.T., Horn, P., Lee, K.H., 2011. Multimodality imaging in the surgical treatment of children with nonlesional epilepsy. Neurology 76, 41–48.

Soares, B.P., Porter, S.G., Saindane, A.M., Dehkharghani, S., Desai, N.K., 2016. Utility of double inversion recovery MRI in paediatric epilepsy. Br. J. Radiol. 89, 20150325.
Stehling, C., Vieth, V., Bachmann, R., Nassenstein, I., Kugel, H., Kooijman, H., Heindel, W., Fischbach, R., 2007. High-resolution magnetic resonance imaging of the temporomandibular joint: image quality at 1.5 and 3.0 Tesla in volunteers. Investig. Radiol. 42, 428–434.
Tanner, M., Gambarota, G., Kober, T., Krueger, G., Erritzoe, D., Marques, J.P., Newbould, R., 2012. Fluid and white matter suppression with the MP2RAGE sequence. J. Magn. Reson. Imaging 35, 1063–1070.
Taylor, D.C., Falconer, M.A., Bruton, C.J., Corsellis, J.A., 1971. Focal dysplasia of the cerebral cortex in epilepsy. J. Neurol. Neurosurg. Psychiatry 34, 369–387.
Tschampa, H.J., Urbach, H., Malter, M., Surges, R., Greschus, S., Gieseke, J., 2015. Magnetic resonance imaging of focal cortical dysplasia: comparison of 3D and 2D fluid attenuated inversion recovery sequences at 3 T. Epilepsy Res. 116, 8–14.
Tsutsumi, S., Ito, M., Yasumoto, Y., Tabuchi, T., Ogino, I., 2011. The Virchow-Robin spaces: delineation by magnetic resonance imaging with considerations on anatomofunctional implications. Childs Nerv. Syst. 27, 2057–2066.
Wang, I., Alexopoulos, A., 2016. MRI postprocessing in presurgical evaluation. Curr. Opin. Neurol. 29, 168–174.
Wang, D.D., Deans, A.E., Barkovich, A.J., Tihan, T., Barbaro, N.M., Garcia, P.A., Chang, E.F., 2013a. Transmantle sign in focal cortical dysplasia: a unique radiological entity with excellent prognosis for seizure control. J. Neurosurg. 118, 337–344.
Wang, Z.I., Alexopoulos, A.V., Jones, S.E., Jaisani, Z., Najm, I.M., Prayson, R.A., 2013b. The pathology of magnetic-resonance-imaging-negative epilepsy. Mod. Pathol. 26, 1051–1058.
Wang, Z.I., Suwanpakdee, P., Jones, S.E., Jaisani, Z., Moosa, A.N., Najm, I.M., von Podewils, F., Burgess, R.C., Krishnan, B., Prayson, R.A., Gonzalez-Martinez, J.A., Bingaman, W., Alexopoulos, A.V., 2016. Re-review of MRI with post-processing in nonlesional patients in whom epilepsy surgery has failed. J. Neurol. 263, 1736–1745.
Woermann, F.G., Vezina, G., 2013. Structural imaging in children with chronic focal epilepsy: diagnostic algorithms and exploration strategies. Handb. Clin. Neurol. 111, 747–757.
Wong-Kisiel, L.C., Britton, J.W., Witte, R.J., Kelly-Williams, K.M., Kotsenas, A.L., Krecke, K.N., Watson Jr., R.E., Patton, A., Hanson, D.P., Mandrekar, J., 2016. Double inversion recovery magnetic resonance imaging in identifying focal cortical dysplasia. Pediatr. Neurol. 61, 87–93.